Proceedings of the 2nd International Conference on Applied Physics and Mathematical Modeling
DOI: 10.54254/2753-8818/95/2024.21242

Research on Trajectory Control of Large Aircraft in Wind Shear Based on Mathematical Models

Ziyao Hu

School of Electronics and Information Engineering, Liaoning Technical University, Huludao, Liaoning

3311614471@qq.com

Abstract. To address the impact of low-altitude wind shear on aircraft flight safety, this paper establishes a real-time low-altitude headwind shear model based on the vortex ring method and an aircraft dynamic model incorporating disturbance wind parameters. The study investigates the effects of wind shear on aircraft and proposes both longitudinal and lateral escape strategies. In the simulation study, vertical and horizontal wind vector fields of wind shear were first simulated, and wind shear vector diagrams were plotted. Then, using the B747-100 aircraft as the research object, a longitudinal escape numerical simulation was conducted at 80 seconds by setting relevant parameters, followed by a lateral escape simulation at 45 seconds. The results indicate that low-altitude wind shear can lead to a decrease in aircraft airspeed, significant changes in pitch angle, and a reduction in flight altitude, thereby increasing the risk of a crash. Additionally, when encountering wind shear, implementing a longitudinal escape strategy (maintaining a 15° pitch angle and full thrust) can effectively recover flight altitude. The lateral escape strategy also successfully allows the aircraft to escape wind shear. This research provides theoretical foundations and technical support for enhancing aviation flight safety.

Keywords: vortex ring model, dynamic model with disturbance wind parameters, six degrees of freedom, escape strategy.

1. Introduction

Low-altitude wind shear refers to the phenomenon where wind speed and direction undergo significant changes within a relatively short distance or time below an altitude of 600 meters, posing a serious threat to aircraft operational safety [1]. By establishing wind shear models and aircraft dynamic models, it is possible to analyze the impact of wind shear on the flight state of an aircraft in real-time and explore appropriate handling methods to reduce the probability of a crash.

Michael Ivan [2] constructed a microburst model based on the vortex ring principle, simplifying the simulation model. Gao Zhenxing [3] researched the modeling methods of three-dimensional microburst wind shear based on the vortex ring and composite vortex principles, improving the vortex ring model to better match actual wind field conditions. The aerodynamic model established by Gao Zhenxing [3] is a quasi-steady aerodynamic model based on a first-order linear approximation, with corrections made to certain aerodynamic derivative terms. Gui Yuanyang [4] studied microbursts based on the Soesman model, enhancing the realism of aircraft flight state simulations. Fu Peng [5] designed an automatic landing controller for passenger aircraft using the PID linear control method, enabling the aircraft to

DOI: 10.54254/2753-8818/95/2024.21242

successfully traverse low-altitude wind shear with robust performance. Caiyan Lin et al. [6] studied the characteristics of low-altitude wind shear in mainland China, finding that it primarily occurs below 600 meters in altitude and is closely related to complex terrain and weather conditions. Afaq Khattak et al. [7] used Bayesian optimization and ensemble learning classifiers to predict key aspects of low-altitude wind shear, providing important references for airport management.

In light of this, this paper establishes a microburst wind shear model and a dynamic model incorporating disturbance wind parameters to study the impact of wind vectors on aircraft flight and proposes effective longitudinal and lateral escape strategies. The research in this paper provides a theoretical basis for enhancing aviation flight safety.

2. Model Principles

2.1. Low-Altitude Headwind Shear Model

In this paper, the real-time low-altitude headwind shear model is established using the vortex ring method proposed by Michael Ivan. The runway coordinate system is set with the runway threshold as the origin and the approach direction as the $+X_R$ axis, as shown in Figure 1.

The primary vortex ring curve equation, with a vortex ring radius of R, is located above the ground at point $\boldsymbol{O_P}(x_a, y_a, z_a)^T$:

$$\begin{cases} (x - x_P)^2 + (y - y_P)^2 = R^2 \\ z = z_P \end{cases} \tag{1}$$

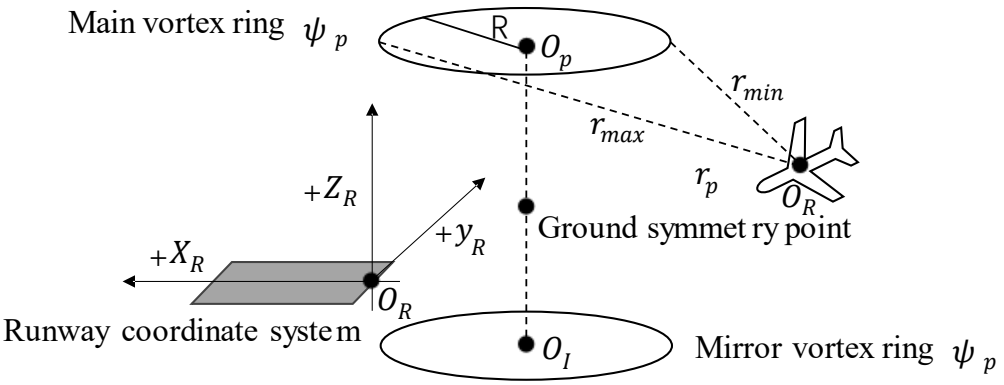

Figure 1. Vortex Ring Model in the Runway Coordinate System

The streamline equation is given by $\psi_P = \frac{\Gamma}{2\pi}(r_{max} + r_{min})F(k)$, where the vortex ring strength $\Gamma = 2RW_{z0}$, with W_{z0} representing the pre-set vertical velocity at the vortex ring center. The terms r_{max} and r_{min} denote the maximum and minimum distances from any point $\boldsymbol{O_A}$ in space to the primary vortex ring. $F(k)$ represents the elliptical integral function, where $k = \left|\frac{r_{max} - r_{min}}{r_{max} + r_{min}}\right|$. When $0 \le k \le 1$, $F(k)$ can be approximated as $F(k) \approx \frac{0.778k^2}{0.25 + 0.75\sqrt{1-k^2}}$.

From the streamline equation, the corresponding radial induced velocity at point relative to the primary vortex ring is given by $w_r^P = \frac{1}{r_P}\frac{\partial \psi_P}{\partial z_R}$, and the axial induced velocity is $w_z^P = -\frac{1}{r_P}\frac{\partial \psi_P}{\partial r_p}$, where r_P is the distance from point $\boldsymbol{O_A}$ to the vortex ring axis. The radial velocity components in the x_R and y_R directions can be expressed as $w_x^P = \frac{x_A - x_P}{r_P} w_r^P$ and $w_y^P = \frac{y_A - y_P}{r_P} w_r^P$. To ensure that the vertical wind vector at the ground level is zero, a mirror vortex ring is configured such that the wind vectors of the primary vortex ring and the mirror vortex ring are equal in magnitude but opposite in direction at

DOI: 10.54254/2753-8818/95/2024.21242

the ground. The induced velocities w_x^I、w_y^I、w_z^I at point $\boldsymbol{O_A}$ due to the mirror vortex ring are then obtained. The combined induced velocity from the two vortex rings at $\boldsymbol{O_A}$ is:

$$\begin{pmatrix} W_x \\ W_y \\ W_z \end{pmatrix} = \begin{pmatrix} w_x^P \\ w_y^P \\ w_z^P \end{pmatrix} + \begin{pmatrix} w_x^I \\ w_y^I \\ w_z^I \end{pmatrix} \tag{2}$$

Additionally, for points where $r_P = 0$ or where $r_P = R$ and $z_A = z_P$, the induced velocities are infinite.

2.2. Dynamic Model Incorporating Disturbance Wind Parameters

To study the impact of microburst disturbance wind vectors $\boldsymbol{W} = (W_x, W_y, W_z)^T$ on aircraft flight [3], it is necessary to establish the state equations describing the aircraft's motion in the air. From the body coordinate system shown in Figure 2, the equations of motion for the aircraft's center of mass are derived as follows:

$$\begin{cases} \dot{V}_x = \dfrac{X}{m} - \dot{W}_{xB} - g\,sin\theta - \left[q(V_x + W_{zB}) - r\left(V_y + W_{yB}\right)\right] \\ \dot{V}_y = \dfrac{Y}{m} - \dot{W}_{yB} + g\,sin\phi cos\theta - [r(V_x + W_{xB}) - p(V_z + W_{zB})] \\ \dot{V}_z = \dfrac{Z}{m} - \dot{W}_{zB} + g\,cos\phi cos\theta - \left[p\left(V_y + W_{yB}\right) - q(V_x + W_{xB})\right] \end{cases} \tag{3}$$

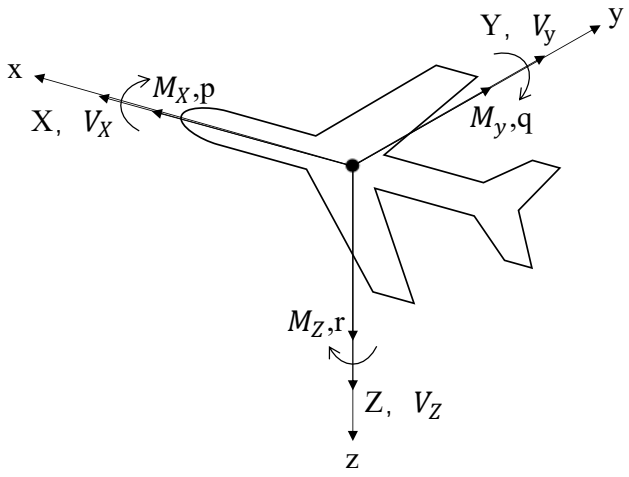

Figure 2. Six-Degrees-of-Freedom Aircraft Motion (Body Coordinate System)

Here, g represents gravitational acceleration, q is the pitch rate, r is the yaw rate, and p is the roll rate. The relationship between airspeed V and the velocity components in the body frame is given by: $V = \sqrt{V_x^2 + V_y^2 + V_z^2}$. The angle of attack α and the sideslip angle β are calculated as: $\alpha = \arctan\left(\frac{V_z}{V_x}\right)$, $\beta = \arcsin\left(\frac{V_y}{V}\right)$.

By solving for the roll angle $\dot{\phi}$, pitch angle $\dot{\theta}$, and yaw angle $\dot{\psi}$, the kinematic equations are obtained.

$$\begin{cases} \dot{\phi} = p + \tan\theta(q\sin\phi + r\cos\phi) \\ \dot{\theta} = q\cos\phi - r\sin\phi \\ \dot{\psi} = \dfrac{(q\sin\phi + r\cos\phi)}{\cos\theta} \end{cases} \tag{4}$$

DOI: 10.54254/2753-8818/95/2024.21242

The equations of rotational motion in the body coordinate system and the navigation equations considering the effects of disturbance winds can be referenced from [3].

When the aircraft is flying in the vertical plane, the sideslip angle $\beta = 0$, roll angle $\phi = 0$, yaw angle $\psi = 0$, side force $Y = 0$, roll moment $M_x = 0$, and yaw moment $M_z = 0$. Consequently, the dynamic equations from Section 1.2 can be simplified into six equations. After some simplification, the reduced set of three-degree-of-freedom dynamic equations that describe the longitudinal flight of the aircraft are obtained as follows:

$$\begin{cases} \dot{V}_x = \dfrac{X}{m} - \dot{W}_{xB} - g\sin\theta - q(V_z + W_{zB}) \\ \dot{V}_z = \dfrac{Z}{m} - \dot{W}_{zB} - g\cos\phi\cos\theta + q(V_x + W_{xB}) \\ \dot{\theta} = q \\ I_y\dot{q} = M_y \\ \dot{x}_E = V_x\cos\theta + V_z\sin\theta + W_x \\ \dot{z}_E = V_x\sin\theta - V_z\cos\theta + W_z \end{cases} \tag{5}$$

The aircraft's flight state in the air can be simplified as $x = [V, \alpha, \theta, q, x, H]^T$, with the corresponding control inputs as $u = [\delta_t, \delta_e]^T$.

3. Simulation Study

3.1. Data Preprocessing

In this study, the B747-100 aircraft is selected as the research subject. Its structural parameters are shown in Table 1.

Table 1. Structural Parameters of the B747-100 Aircraft

Parameter (Unit)	Value	Parameter (Unit)	Value
Wing Area S(m^2)	511	Aircraft Weight b(m)	59.64
Mean Aerodynamic Chord $\overline{c}$(m)	8.32	Aerodynamic Center Position x_{cg}	$0.25\overline{c}$
Moment of Inertia about x-axis I_x(kg·m^2)	1.92×10^7	Moment of Inertia about y-axis I_x(kg·m^2)	4.38×10^7
Moment of Inertia about z-axis I_z(kg·m^2)	6.15×10^7	Product of Inertia I_{xz}(kg·m^2)	1.18×10^7
Aircraft Weight m(kg)	2.73×10^5		

To facilitate the simulation study, a 4th-5th order Runge-Kutta numerical integration algorithm is employed to calculate real-time flight state parameters. Additionally, the aircraft's dynamic model is trimmed for equilibrium.

3.2. Parameter Settings and Simulation Analysis

1) Simulation of the Impact of Low-Altitude Wind Shear on Flight State

Using the runway coordinate system shown in Figure 1, the microburst vortex ring center is set at $\boldsymbol{O_P} = (-2000\ 0\ 600)^T$ meters, with a vortex ring radius $R = 600$ meters, a vortex core radius $r = 450$ meters, and a vertical wind speed at the vortex center $W_{z0} = 10$ m/s. The wind vector field obtained from the simulation is illustrated in Figure 3.

DOI: 10.54254/2753-8818/95/2024.21242

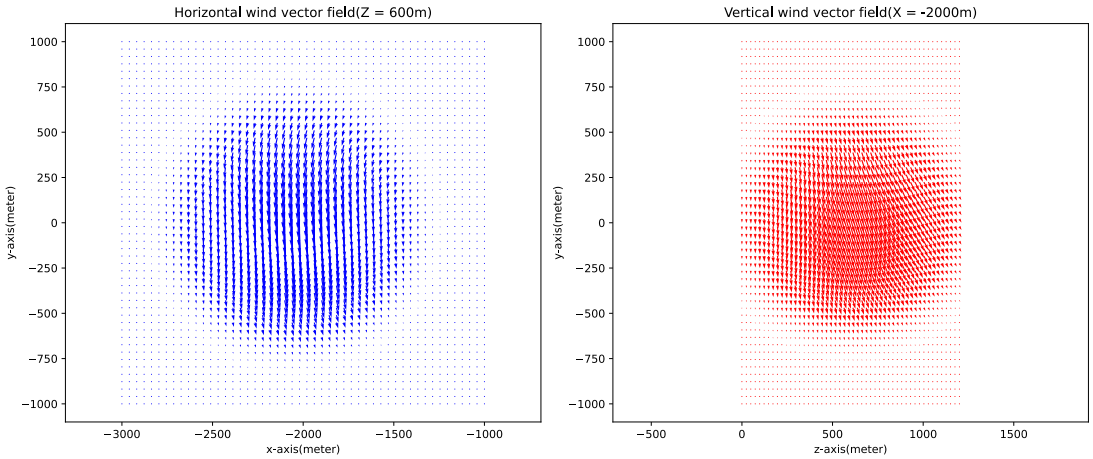

Figure 3. Wind Vector Diagram in Wind Shear

In the horizontal wind vector field at a height of 600 meters, there is a strong horizontal vortex, with wind speed strongest at the center and gradually weakening outward. In the vertical wind vector field at $x = -2000m$, the vertical wind speed is strongest at the center, gradually decreasing outward.

Taking approach and landing as an example, a real-time numerical simulation is conducted to analyze the aircraft's disturbed flight state under microburst wind shear. The results are shown in Figure 4.

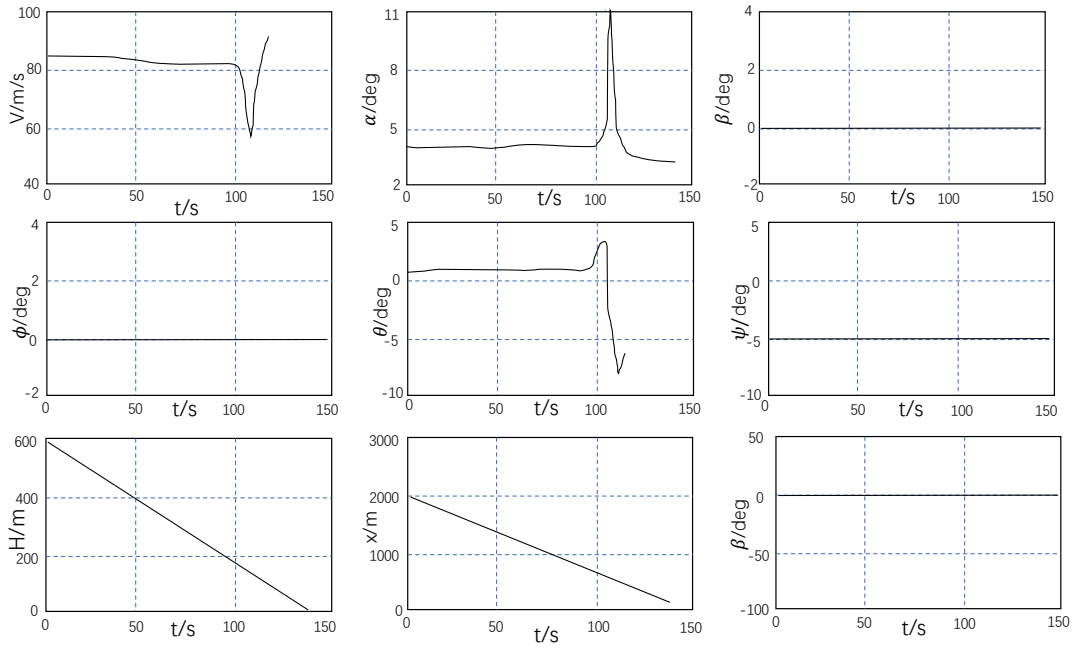

Figure 4. Aircraft Passing Through a Microburst Without Control

From the analysis of Figure 4, it can be observed that low-altitude headwind shear causes a decrease in airspeed, with the angle of attack and pitch angle undergoing drastic changes before reducing. The aircraft's altitude also experiences a sharp decline, indicating that the aircraft is subjected to strong airflow effects in the vertical direction. The simulation results demonstrate that microbursts have a significant impact on the aircraft's flight state, especially during the approach and landing phase, where the aircraft's stability is severely challenged.

2) Simulation of Aircraft Recovery Strategies

DOI: 10.54254/2753-8818/95/2024.21242

a. Simulation of Longitudinal Recovery from Wind Shear

The FAA suggests three methods for dealing with microbursts, one of which involves passing through the wind field at a 15° pitch angle when the angle of attack has not yet reached the critical angle. Using the B747 aircraft during descent as an example, the initial velocity is set to $V = 79m/s$, and the aircraft begins climbing from an altitude of $500m$ with a flight path angle γ=7deg. The initial flight state is trimmed and simulated dynamically, resulting in the initial state parameters $\alpha = 0.22deg$ and $\theta = 5.22deg$. The initial control parameters are $\delta_t = 0.833313$ and $\delta_e = -14.0085$. Assuming the aircraft begins longitudinal recovery control at 80 seconds, the simulation results are plotted.

From the simulation results shown in Figure 5, the effect of the B747 aircraft's longitudinal recovery strategy when encountering a microburst can be analyzed in detail: With full throttle applied, the aircraft's speed gradually increases from 79 m/s and rapidly accelerates to approximately 120 m/s after 80 seconds due to wind shear. The initial pitch angle of 5.22° is adjusted to nearly 20° at 80 seconds to maintain the target pitch angle of 15°, ensuring safe passage through the wind field. The aircraft's altitude drops from 500 meters to approximately 200 meters to avoid the hazardous region caused by the wind shear.

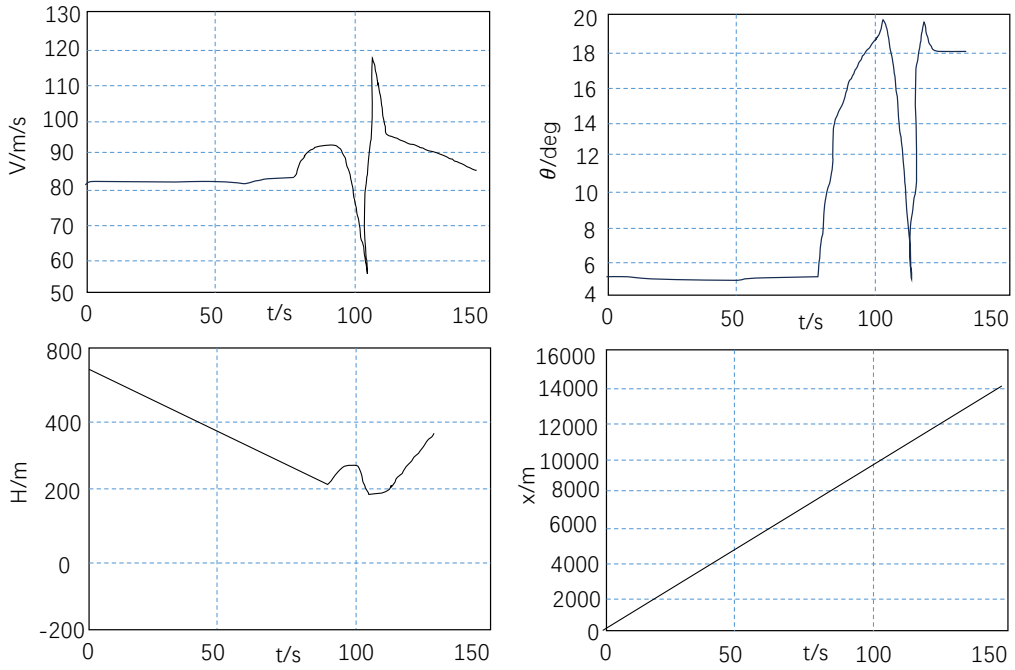

Figure 5. Aircraft Longitudinal Recovery from Microburst

b. Simulation of Lateral Recovery from Wind Shear

Adjusting from the weaker wind side of the wind field is also an effective strategy when encountering a microburst. Using the B747 aircraft during the final approach as an example, the glide path altitude is set to 600 meters, with an approach speed ranging from 66.9 m/s to 77.2 m/s and a flight path angle of -2.5deg~-3deg. Trimming results in a glide speed of 150 m/s, an altitude $H = 600$ meters, and a flight path angle $\gamma = -2.5\text{deg}$. The initial aircraft state parameters are set to $\alpha = 0.6589\text{deg}$ and $\theta = -1.8411\text{deg}$. The initial control parameters obtained are $\delta_t = 0.303076$ and $\delta_e = -15.8112$.

At 45 seconds, the aircraft is set to turn left to avoid the wind shear. The simulation results are plotted in Figure 6.

DOI: 10.54254/2753-8818/95/2024.21242

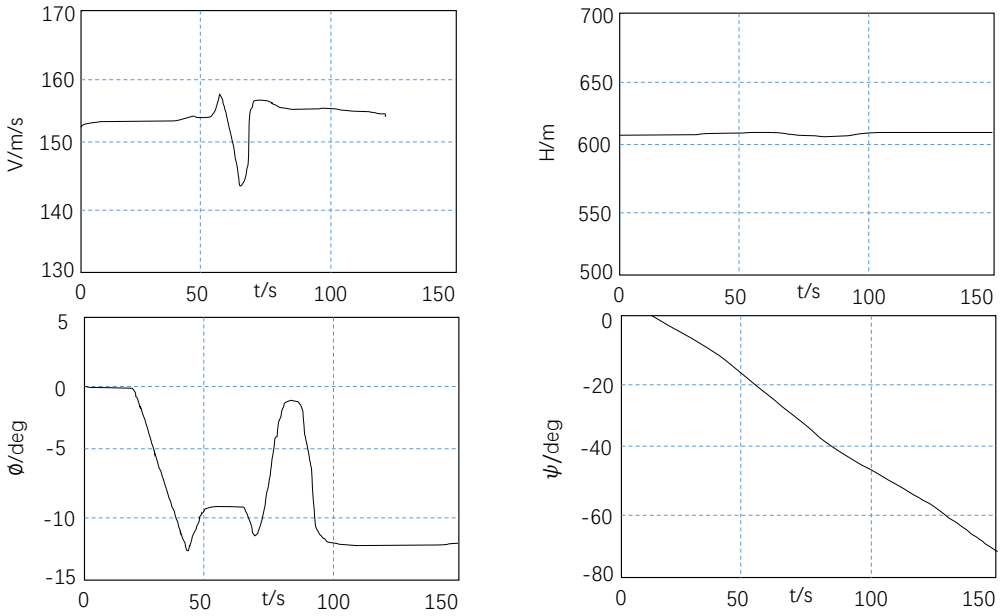

Figure 6. Aircraft Lateral Recovery from Microburst

From the simulation results in Figure 6, the effect of the B747 aircraft's lateral recovery strategy when encountering a microburst can be analyzed in detail: The initial speed of the aircraft is approximately 150 m/s, which significantly decreases around 50 seconds, and then recovers, indicating that the speed is affected during lateral recovery. The aircraft maintains an altitude of 600 meters. The roll angle ϕ rapidly changes from 0° to approximately -12° around 35 seconds, followed by significant fluctuations, eventually stabilizing at -12°. The yaw angle ψ changes linearly. These results indicate that the aircraft undergoes significant yaw adjustments during lateral recovery.

4. Conclusion

Numerical simulations indicate that low-altitude wind shear significantly affects an aircraft's flight status, leading to changes in airspeed, angle of attack, and altitude, thereby increasing the risk of ground impact. During the simulations, the aircraft's airspeed rapidly increased from 79 m/s to approximately 120 m/s, the angle of attack adjusted from 5.22° to nearly 20°, and the altitude dropped from 500 meters to about 200 meters, highlighting the intense impact of the airflow.

Therefore, implementing correct recovery strategies is crucial. The longitudinal recovery strategy, which maintains a 15° pitch angle and full throttle, effectively increases the speed from 79 m/s to 120 m/s and recovers altitude, but care must be taken to ensure the angle of attack does not exceed the critical value. The lateral recovery strategy, which adjusts from the weaker wind side, shows that the speed initially decreases around 50 seconds but then recovers. The roll angle changes from 0° to -12°, and the yaw angle varies linearly, helping to avoid the wind shear region.

In summary, low-altitude wind shear has a significant impact on flight status, and proper recovery strategies are essential to ensure flight safety. Simulation validation demonstrates that both longitudinal and lateral recovery strategies can effectively counter microbursts, ensuring the safe flight of the aircraft.

References

[1] We, J., & Sun, R. (2021). Study on the impact of low-altitude wind shear on aircraft performance [Conference paper]. In Chinese Society of Aeronautics and Astronautics (Ed.), Proceedings of the 5th China Aviation Science and Technology Conference (p. 6). Civil Aviation University of China, School of Economics and Management; Civil Aviation University of China, Flight College. https://doi.org/10.26914/c.cnkihy.2021.064857

DOI: 10.54254/2753-8818/95/2024.21242

[2] Zhang, R. (2012). Modeling, hazard detection, and control law research of large aircraft under low-altitude wind shear [Doctoral dissertation, Shanghai Jiao Tong University].

[3] Gao, Z. (2009). Real-time simulation modeling of large aircraft flight under complex atmospheric disturbances [Doctoral dissertation, Nanjing University of Aeronautics and Astronautics].

[4] Gui, Y. (2013). Research on automatic landing safety control strategies for aircraft under low-altitude wind shear [Doctoral dissertation, Nanjing University of Aeronautics and Astronautics].

[5] Fu, P. (2016). Warning and control research for passenger aircraft under low-altitude wind shear [Doctoral dissertation, Nanjing University of Aeronautics and Astronautics].

[6] Lin, C., Zhang, K., Chen, X., Liang, S., Wu, J., & Zhang, W. (2021). Overview of low-level wind shear characteristics over Chinese mainland. Atmosphere, 12(5), Article 628. https://doi.org/10.3390/atmos12050628

[7] Khattak, A., Chan, P.-W., Chen, F., & Peng, H. (2022). Prediction and interpretation of low-level wind shear criticality based on its altitude above runway level: Application of Bayesian optimization–ensemble learning classifiers and SHapley additive explanations. Atmosphere, 13(12), Article 2102. https://doi.org/10.3390/atmos13122102